

Quaternary Jordan-Wigner mapping and topological extended-kink phase in the interacting Kitaev ring

Zhen-Yu Zheng,^{1,2} Han-Chuan Kou,^{1,2} and Peng Li^{1,2,*}

¹College of Physics, Sichuan University, 610064, Chengdu, P. R. China

²Key Laboratory of High Energy Density Physics and Technology of Ministry of Education, Sichuan University, 610064, Chengdu, P. R. China

(Dated: December 15, 2024)

On a ring, a single Jordan-Wigner transformation between the Kitaev model and the spin model suffers redundant degrees of freedom. However, we can establish a complete quaternary Jordan-Wigner mapping involving two Kitaev rings and two spin rings with periodic or antiperiodic boundary conditions in the transverse direction. This mapping facilitates us to demonstrate exactly how a topological extended-kink (TEK) phase develops in the interacting Kitaev ring with geometrical ring frustration. Unlike the usual topological phases protected by energy gap in noninteracting systems, this topological phase is gapless. And because the spectra of low energy excitations are quadratic, the specific heat per site approaches a half of Boltzmann constant near absolute zero temperature. More important, the ground state is unique, immune to spontaneous symmetry breaking, and exhibits long-range correlation but without local order parameter. We also demonstrate that concomitant localized kink zero modes (KZM's) take place by introducing a type of bond defect.

Introduction.—Interacting Kitaev chain attracts more and more attention recently [1–5]. It was pointed out that the classification of topological phases in noninteracting fermionic systems [6, 7] may not apply to the interacting ones [1]. At a symmetric point, Miao *et al.* found the problem can be solved exactly by a scheme of two-step Jordan-Wigner transformations (JWT's) [8]. And plentiful phases have been disclosed in the dimerized case [9–11]. On the other hand, geometrical frustration first introduced in the classical Ising spin systems plays an important role in quantum antiferromagnetism [12]. The concept of frustration can be generalized to fermionic systems with quantum noncommutativity, because similar effect of quantum entanglement arises even without geometrical frustration [13–19].

In this work, we first point out how a quaternary Jordan-Wigner mapping links two Kitaev rings and two spin rings with periodic or antiperiodic boundary conditions, then solve an interacting Kitaev ring at the symmetric point [8]. We only consider the total number of lattice sites $N \in \text{odd}$, which ensures the effect of geometrical ring frustration (RF) [20–27]. A novel topologically nontrivial phase and concomitant zero modes emerge due to the interplay between RF and quantum fluctuations.

Quaternary Jordan-Wigner mapping.—It is known [28] that the Kitaev chain with open boundary condition (OBC),

$$H_{\text{OBC}}(c) = \sum_{j=1}^{N-1} [(-tc_j^\dagger c_{j+1} + \Delta c_j c_{j+1} + \text{h.c.}) + U(2n_j - 1)(2n_{j+1} - 1)] - \sum_{j=1}^N \mu(2n_j - 1), \quad (1)$$

can be mapped to the spin XYZ chain with OBC exactly,

$$H_{\text{OBC}}(c) \equiv H_{\text{OBC}}(\sigma) = \sum_{j=1}^{N-1} \left(-\frac{t+\Delta}{2} \sigma_j^x \sigma_{j+1}^x - \frac{t-\Delta}{2} \sigma_j^y \sigma_{j+1}^y + U \sigma_j^z \sigma_{j+1}^z \right) - \sum_{j=1}^N \mu \sigma_j^z, \quad (2)$$

by the Jordan-Wigner transformation (JWT),

$$c_j^\dagger = \frac{1}{2}(\sigma_j^x + i\sigma_j^y) \prod_{l=1}^{j-1} (-\sigma_l^z), \quad (1 \leq j \leq N). \quad (3)$$

In the above, $c = \{c_j, (j = 1, 2, \dots, N)\}$ denotes all fermions residing on the lattice sites, $n_j = c_j^\dagger c_j$, and $\sigma = \{\sigma_j^a, (j = 1, 2, \dots, N; a = x, y, z)\}$ all Pauli spins.

By seaming the open chains with boundary terms,

$$H_b(c, \xi) = \xi(-tc_N^\dagger c_1 + \Delta c_N c_1 + \text{h.c.}) + U(2n_N - 1)(2n_1 - 1), \quad (4)$$

$$H_b(\sigma, \eta) = \eta \left(-\frac{t+\Delta}{2} \sigma_N^x \sigma_1^x - \frac{t-\Delta}{2} \sigma_N^y \sigma_1^y \right) + U \sigma_N^z \sigma_1^z, \quad (5)$$

for the Kitaev chain and the spin chain respectively, we get four distinct Hamiltonians with periodic boundary condition (PBC) or anti-PBC,

$$H_{\text{R/NS}}(c) = H_{\text{OBC}}(c) + H_b(c, \xi), \quad (6)$$

$$H_{\text{P/A}}(\sigma) = H_{\text{OBC}}(\sigma) + H_b(\sigma, \eta). \quad (7)$$

In Eq. (6), the subscript R and NS represent the PBC ($\xi = 1$ or $c_{N+1} = c_1$, the "Ramond" sector) and the anti-PBC ($\xi = -1$ or $c_{N+1} = -c_1$, the "Neveu-Schwarz" sector) respectively [29]. Likewise, in Eq. (7), the subscripts P and A represent the PBC ($\eta = 1$ or $\sigma_{N+1}^a = \sigma_1^a$ ($a = x, y, z$)) and anti-PBC in the transverse direction ($\eta = -1$ or $\sigma_{N+1}^a = -\sigma_1^a$ ($a = x, y$) and $\sigma_{N+1}^z = \sigma_1^z$) respectively.

The boundary terms screw up the mapping between a Kitaev ring and a spin ring through a single JWT [30] due to the mismatch of partial degrees of freedom (DOF) [23].

*Electronic address: lipeng@scu.edu.cn

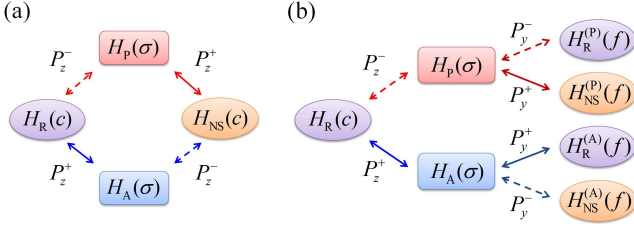


FIG. 1: (Color online) (a) Illustration of the quaternary Jordan-Wigner mapping expressed by Eqs. (8) and (9). (b) The scheme of two-step Jordan-Wigner transformations for solving the Kitaev ring, $H_R(c)$, at the symmetric point. Six auxiliary Hamiltonians are involved.

However, we can fortunately establish a full *quaternary Jordan-Wigner mapping* consisting of four identities,

$$H_{R/NS}(c) = P_z^+ H_{A/P}(\sigma) P_z^+ + P_z^- H_{P/A}(\sigma) P_z^-, \quad (8)$$

$$H_{P/A}(\sigma) = P_z^+ H_{NS/R}(c) P_z^+ + P_z^- H_{R/NS}(c) P_z^-, \quad (9)$$

where $P_z^\pm = \frac{1}{2}(\hat{1} \pm \mathcal{P}_z)$ are projectors with the parity operator $\mathcal{P}_z = \exp(i\pi M_z)$ and $M_z = \sum_{j=1}^N c_j^\dagger c_j = \sum_{j=1}^N (1 + \sigma_j^z)/2$. In fact, $H_P(\sigma)$ with $U = 0$ had been solved through the identity in Eq. (9) [31]. The mapping is illustrated in Fig. 1(a), in which each arrow represents a valid parity channel. Notice that the full mapping runs out of all DOF of the four Hamiltonians. We also notice that the two Kitaev rings can be transformed to each other, $\mathcal{C}^\dagger H_R(c) \mathcal{C} = H_{NS}(c)$, by the particle-hole conjugation operator $\mathcal{C} = \prod_{j=1}^N [c_j^\dagger + (-1)^j c_j]$ when $\mu = 0$.

Exact solution of the Kitaev ring $H_R(c)$ with RF at the symmetric point.—Now we aim at the periodic Kitaev ring $H_R(c)$ at the symmetric point $\mu = 0$ and $t = \Delta$. It can be exactly solved by a scheme of two-step JWT's similar to the one for OBC problem [8]. The scheme is shown in Fig. 1 (b). By the first step of JWT, Eq. (3), the resulting Hamiltonians, $H_P(\sigma)$ and $H_A(\sigma)$, are spin XZ rings. In the second step, we perform the JWT,

$$f_j^\dagger = \frac{1}{2}(\sigma_j^z + i\sigma_j^x) \prod_{l=1}^{j-1} (-\sigma_l^y), \quad (10)$$

for $H_P(\sigma)$ and another JWT,

$$f_j^\dagger = \frac{1}{2}[\sigma_j^z + i(-1)^{j+1}\sigma_j^x] \prod_{l=1}^{j-1} (-\sigma_l^y), \quad (11)$$

for $H_A(\sigma)$ respectively, so as to get four Hamiltonians,

$$H_s^{(P)}(f) = H(s, -t + U, t + U), \quad (12)$$

$$H_s^{(A)}(f) = H(s, t + U, -t + U), \quad (13)$$

where s refers to R or NS. Appropriate parameters are to be substituted into the general free fermion Hamiltonian [33, 34],

$$H(s, a, b) = \sum_{q \in Q_s, q \neq q_s} \phi_q^\dagger (h_y \sigma^y + h_z \sigma^z) \phi_q + a \cos q_s (2f_{q_s}^\dagger f_{q_s} - 1), \quad (14)$$

with $\phi_q^\dagger = (f_q^\dagger, f_{-q})$, Pauli matrices σ^y and σ^z , $h_y = -b \sin q$, $h_z = -a \cos q$, $q_R = 0$, $q_{NS} = \pi$, and

$$Q_R = \left\{ -\frac{N-1}{N}\pi, \dots, -\frac{2}{N}\pi, 0, \frac{2}{N}\pi, \dots, \frac{N-1}{N}\pi \right\}, \quad (15)$$

$$Q_{NS} = \left\{ -\frac{N-2}{N}\pi, \dots, -\frac{1}{N}\pi, \frac{1}{N}\pi, \dots, \frac{N-2}{N}\pi, \pi \right\}. \quad (16)$$

The associated projectors are $P_y^\pm = \frac{1}{2}(\hat{1} \pm \mathcal{P}_y)$ and parity operator is $\mathcal{P}_y = \exp(i\pi M_y)$ with $M_y = \sum_{j=1}^N f_j^\dagger f_j = \sum_{j=1}^N (1 + \sigma_j^y)/2$. At last, the solution of $H_R(c)$ is retrieved by filtering out redundant DOF of the auxiliary Hamiltonians following the scheme in Fig. 1(b) (Appendix A).

Ground-state phase diagram and spectra of low energy excitations.—In the parameter range $t > 0$ and $-\infty < U < \infty$, the ground state is of odd parity and reads

$$|E_0\rangle = \frac{1}{\sqrt{2}}(f_0^\dagger |\phi_R^{(P)}\rangle - |\phi_{NS}^{(P)}\rangle), \quad (17)$$

where $|\phi_R^{(P)}\rangle$ and $|\phi_{NS}^{(P)}\rangle$ are BCS-type vacua of $H_R^{(P)}(f)$ and $H_{NS}^{(P)}(f)$ respectively. In the thermodynamic limit, $N \rightarrow \infty$, there are two phase transition points occurring at $U = \pm t$. Three phases emerge (Fig. 2): the Schrödinger-cat-like (CAT), topological superconductor (TSC), and topological extended-kink (TEK) states. In the CAT phase, another energy level with even parity approaches the ground state rapidly with N increasing, so the ground state becomes doubly degenerate. In the TSC and TEK phases, the ground state remains unique. The CAT and TSC are gapped, while the TEK phase becomes gapless surprisingly.

$2N$ low-lying energy levels involve in the gapless TEK phase. We label them as $\{|E_{P/A}(q)\rangle, \forall q \in Q_R\}$, in which $|E_P(0)\rangle \equiv |E_0\rangle$ is exactly the ground state. They come from the two channels, $H_{P/A}(\sigma)$, respectively. As shown in Fig. 2, these low energy excitations form two inter-

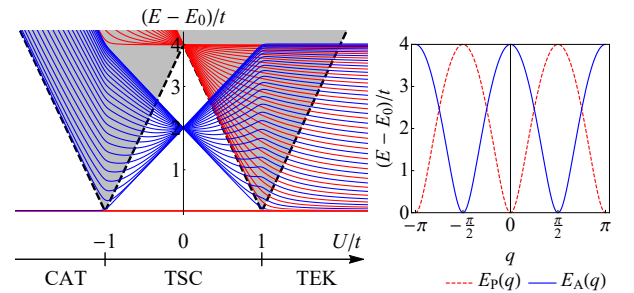


FIG. 2: (Color online) *Left*: Low-lying energy levels and ground-state phase diagram of $H_R(c)$. We choose $N = 51$ for demonstration. The red lines represent levels of odd parity, while the blue ones even parity. All other levels distribute in the shaded area above the dashed line. There are three phases: the Schrödinger-cat-like (CAT), the topological superconducting (TSC), and the topological extended-kink (TEK) phases. Critical points occur at $U = \pm t$. *Right*: The lowest two exact energy spectra in the TEK phase at $U/t = 2$.

weaving true spectra,

$$E_P(q) = 2\omega_P(q) + \mathcal{E}_0 - (U - t), \quad (18)$$

$$E_A(q) = 2\omega_A(q) + \mathcal{E}_0 + |U + t| - 2U, \quad (19)$$

where $\omega_{P/A}(q) = \sqrt{U^2 + t^2 \mp 2Ut \cos(2q)}$ and $\mathcal{E}_0 = (U - t) - \sum_{q \in Q_R} \omega_P(q)$. This newly discovered TEK phase is the main focus of this paper.

Thermodynamics of the TEK phase.—The density of states (DOS) at low energies is determined by the lowest two gapless spectra. It turns out to be divergent near the ground state, $\rho(E - E_0) \sim 1/\sqrt{E - E_0}$, since the spectra are quadratic, $E_P(q) \sim q^2 + (q - \pi)^2$ and $E_A(q) \sim (q - \pi/2)^2 + (q + \pi/2)^2$. So one can find that the specific heat per site approaches a constant when $T \ll 4t/k_B$,

$$C_M/N = \frac{k_B}{2} + \frac{k_B^2(U^2 + Ut + t^2)}{8tU(U - t)}T + O(T^2), \quad (20)$$

where k_B is the Boltzmann constant. This exotic behaviour is in contrast to the linear law in temperature, $C_M/N \sim T$, which goes to zero when $T \rightarrow 0$ no matter there are interactions or not [35].

Entanglement entropy of the ground state.—To reveal the entangled nature of the ground state, let us see the entanglement entropy (EE) [?]. We define the reduced density matrix as $\rho_l = \text{tr}_{N-l} |E_P(0)\rangle \langle E_P(0)|$ and the EE as $S_l = -\text{tr}(\rho_l \log_2 \rho_l)$. The evaluation of EE is performed numerically [23]. The results of $S_{(N-1)/2}$ are illustrated in Fig. 3. We see the TEK phase is highly entangled, but its EE is not divergent although the spectra are gapless.

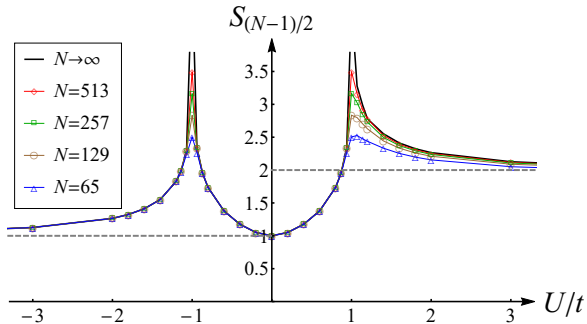


FIG. 3: (Color online) Entanglement entropy (EE), $S_{(N-1)/2}$. The black solid line is an extrapolation to $N \rightarrow \infty$. The two gray dashed lines indicate the lower bound for the CAT and TSC phases ($EE = 1$) and the TEK phase ($EE = 2$). The case for $N \rightarrow \infty$ is obtained by extrapolation from the data of finite $N \in \text{odd}$. At the two critical points, $U/t = \pm 1$, the EE becomes divergent and obeys the CFT's prediction, $S_{(N-1)/2}^c \sim \frac{1}{2} + \frac{1}{3} \log_2 N$ for $N \rightarrow \infty$.

Correlation function of the ground state.—In the Toeplitz determinant representation, we write down the

correlation function for the ground state (Appendix B),

$$\begin{aligned} C_{r,N} &= \langle E_P(0) | (2n_j - 1)(2n_{j+r} - 1) | E_P(0) \rangle \\ &= \frac{1}{2} (\det[\mathcal{D}_{l-m}^{(R)} + \frac{2}{N}]_{1 \leq l, m \leq r} + \det[\mathcal{D}_{l-m}^{(NS)}]_{1 \leq l, m \leq r}), \end{aligned} \quad (21)$$

where $\mathcal{D}_n^{(s)} = -\frac{e^{-iq_s}}{N} e^{-iq_s n} + \frac{1}{N} \sum_{q \in Q_s, q \neq q_s} e^{-iq_n} D(e^{iq})$, $D(e^{iq}) = \frac{-(U - te^{-2iq})}{\sqrt{(U - te^{-2iq})(U - te^{2iq})}}$. The evaluation of the two Toeplitz determinants in Eq. (21) is direct. But one should be very careful to keep the ratio $\alpha = \frac{r}{N}$ before taking the thermodynamic limit $N \rightarrow \infty$, because nonzero α in the expression reflects the system's nonlocal information [27]. With the help of a generalized Szegő's theorem [23, 24], the asymptotic results are obtained and read

$$\begin{aligned} C(r, \alpha) &\equiv \lim_{N \rightarrow \infty} C_{r,N} \\ &\approx \begin{cases} \sqrt{1 - t^2/U^2}, & (U < -t), \\ 0, & (|U| < t), \\ (-1)^r (1 - 2\alpha) \sqrt{1 - t^2/U^2}, & (U > t). \end{cases} \end{aligned} \quad (22)$$

The results for CAT and TSC states are like the ones in OBC problem [8]. However, the correlation for TEK state contains a nonlocal factor [27], $(1 - 2\alpha)$, whose presence signifies the non-existence of local order parameter of the CDW type although the correlation is long-range. This can be visualized in the perturbative theory below.

Extended-kink states: perspective from a perturbative theory.—To comprehend what the TEK phase is, let us see a perturbative theory. First, we take the interacting term as the dominant part of $H_R(c)$,

$$H_0(c) = \sum_j U(2n_j - 1)(2n_{j+1} - 1). \quad (23)$$

It is in fact a classical Ising ring, whose ground states are $2N$ -fold degenerate. We use these $2N$ classical Ising kink states to span the Hilbert space. Noticing that the c fermion number representation and the spin σ^z representation are identical since $|0_j\rangle = |\downarrow_j\rangle$ and $|1_j\rangle = |\uparrow_j\rangle$, we denote the $2N$ Ising kink states conveniently as

$$|K(j), \uparrow\rangle = |\cdots, \downarrow_{j-1}, \boxed{\uparrow_j, \uparrow_{j+1}}, \downarrow_{j+2}, \cdots\rangle, \quad (24)$$

$$|K(j), \downarrow\rangle = |\cdots, \uparrow_{j-1}, \boxed{\downarrow_j, \downarrow_{j+1}}, \uparrow_{j+2}, \cdots\rangle. \quad (25)$$

Next, we solve the rest of the Hamiltonian, $V(c) = H_R(c) - H_0(c)$, as the perturbation. For convenience, the calculation is carried out on the spin Hamiltonians $H_{P/A}(\sigma)$. Then by employing the parity projection in Eq. (8), we get the $2N$ low energy excited states,

$$|E_P(q)\rangle \approx \frac{1}{\sqrt{N}} \sum_j e^{-iqj} |K(j), \tau\rangle, \quad (26)$$

$$|E_A(q)\rangle \approx \frac{1}{\sqrt{N}} \sum_j e^{-iqj} |K(j), \bar{\tau}\rangle, \quad (27)$$

where $q \in Q_R$, $(\tau, \bar{\tau}) = (\uparrow, \downarrow)$ for $N = 4K + 1$ and $(\tau, \bar{\tau}) = (\downarrow, \uparrow)$ for $N = 4K + 3$. Two corresponding spectra read

$$E_P(q) \approx -(N - 2)U - 2t \cos(2q), \quad (28)$$

$$E_A(q) \approx -(N - 2)U + 2t \cos(2q), \quad (29)$$

which are good approximations to the exact ones in Eqs. (18) and (19). The degeneracy of the $2N$ levels is lifted. They are *extended-kink states* in the perturbative picture. It is easy to check that their correlation functions grasp the nonlocal factor, $(1 - 2\alpha)$. The ground state is nondegenerate and reads $|E_0\rangle = |E_P(0)\rangle$ for $t > 0$. The spontaneous symmetry breaking, occurring for $H_0(c)$, won't occur any longer when $t \neq 0$. So, in this peculiar situation, we could not define local order parameter by the correlation function following the conventional way [32].

Extended ground-state phase diagram for the TEK phases.—Besides the exactly solvable symmetric point $t = \Delta$, there is another one at $t = -\Delta$. The former is linked to spin XZ rings, the latter spin YZ rings. To distinguish the associate TEK phases, we term them "y-TEK" and "x-TEK" phases respectively. With the help of perturbative theory, we can expand the phase diagram for the TEK phases in the $(t/U, \Delta/U)$ -parameter plane ($U > 0$) as shown in Fig. 4. Notice the ground state is of even parity and comes from $H_A(\sigma)$ when $t < 0$.

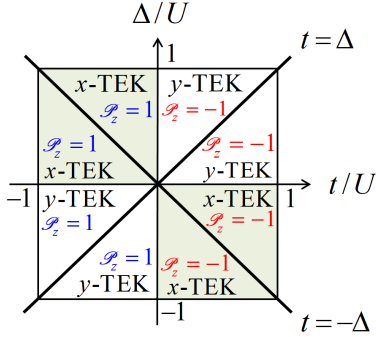


FIG. 4: (Color online) Extended ground-state phase diagram for the TEK phases. Please see details in the text.

Nontrivial topology and localized kink zero modes.—How to manifest the nontrivial topology hidden in the TEK phase? First, we can resort to the four auxiliary noninteracting Kitaev Hamiltonians. We work out the winding number [36] for $H_{R/NS}^{(P)}$,

$$w_P = \int_0^{2\pi} \frac{dq}{2\pi} \frac{h_y \partial_q h_z - h_z \partial_q h_y}{h_y^2 + h_z^2} = \begin{cases} -1, & (U < -t), \\ 1, & (|U| < t), \\ -1, & (U > t). \end{cases} \quad (30)$$

And for $H_{R/NS}^{(A)}$, we obtain $w_A = -w_P$. It seems all phases are topologically nontrivial. But the CAT ($U < -t$) phase will become trivial due to spontaneous symmetry breaking [8]. Unlike the CAT phase, the TSC ($|U| < t$) and TEK ($U > t$) phases maintain nontrivial topology since the ground state is nondegenerate and immune to symmetry breaking.

Second, we can visualize the nontrivial topology of the TEK phase by displaying unconventional zero modes – the localized *kink zero modes* (KZM's). Above all, we can not cut the ring, because the effect of RF will gone.

Let us consider a bond defect by altering the boundary term in $H_R(c)$ as

$$H_b(c, 1) = -t_N(c_N^\dagger c_1 + \text{h.c.}) + \Delta_N(c_N c_1 + \text{h.c.}) + U_N(2n_N - 1)(2n_1 - 1). \quad (31)$$

First, we set uniform interactions, $U_N = U$, so that the effect of RF is maintained and low-energy $2N$ Ising kink states are prepared. Second, we consider the symmetric point, $\Delta = t$ and $\Delta_N = t_N$, so that the defect is controlled by the ratio $\gamma = t_N/t$.

To get a clear picture, we dwell on the reliable perturbative theory proved above. The perturbative treatment is performed on the spin Hamiltonians $H_P(\sigma)$ and $H_A(\sigma)$. Then the solution for $H_R(c)$ is obtained by projection according to Eq. (8). As shown in Fig. 4, we found there emerge two KZM's below the bulk states when $\gamma > 1$. They come from $H_P(\sigma)$ and $H_A(\sigma)$ respectively and read

$$|\text{KZM}_P\rangle = \sum_j \psi_j |K(j), \tau\rangle, \quad (32)$$

$$|\text{KZM}_A\rangle = \sum_j \chi_j |K(j), \bar{\tau}\rangle, \quad (33)$$

where $(\tau, \bar{\tau}) = (\uparrow, \downarrow)$ for $N = 4K + 1$ and $(\tau, \bar{\tau}) = (\downarrow, \uparrow)$ for $N = 4K + 3$ to make sure that $|\text{KZM}_P\rangle$ is of odd parity and $|\text{KZM}_A\rangle$ even parity. Therefore, they are also immune to symmetry breaking. For small N , $|\text{KZM}_A\rangle$ has a little higher energy than $|\text{KZM}_P\rangle$. But with N increasing, they become degenerate rapidly. There is an energy gap, $\Delta_g = t(\gamma - 2 + 1/\gamma)$, from the KZM's to the bulk states. Two features of the KZM's are noticeable:

- (i) ψ_j is symmetric about the bond defect, i.e. $\psi_{N-j} = \psi_j$, while χ_j is antisymmetric, i.e. $\chi_{N-j} = -\chi_j$.
- (ii) For $j < N/2$, we have the asymptotic solution,

$$\psi_j = \chi_j = \begin{cases} \gamma^{-\frac{j+1}{2}} \sqrt{(\gamma^2 - 1)/2}, & (j \in \text{odd}), \\ \gamma^{-\frac{N-j+1}{2}} \sqrt{(\gamma^2 - 1)/2}, & (j \in \text{even}), \end{cases} \quad (34)$$

Thus for $j \in \text{even}$, both ψ_j and χ_j go to zero rapidly with N increasing. While for $j \in \text{odd}$, ψ_j and χ_j approach steady finite values near the defect and make two well localized KZM's. Numerical results for $N = 51$ are illustrated in Fig. 4.

We can also deduce the KZM's from the four auxiliary noninteracting Hamiltonians $H_{R/NS}^{(P)/(A)}(f)$. Then the occurrence of KZM's can be attributed to the boundaries of Katsura's type [34]. So the KZM's can be taken as a special kind of Majorana zero mode crimped in the ring.

Several ways can be utilized to modulate the KZM's. For one example, since $|\text{KZM}_P\rangle$ and $|\text{KZM}_A\rangle$ have opposite parity, a nonzero chemical potential μ can split the two KZM's with a gap proportional to μ . For another example, one can put the parameters to a limiting situation, $t = 0$ and $t_N \gg U$, so as to realize two simpler KZM's with only two components,

$$|\text{KZM}_P\rangle \sim (\psi_1, \psi_{N-1}) = \frac{1}{\sqrt{2}}(1, 1), \quad (35)$$

$$|\text{KZM}_A\rangle \sim (\chi_1, \chi_{N-1}) = \frac{1}{\sqrt{2}}(1, -1). \quad (36)$$

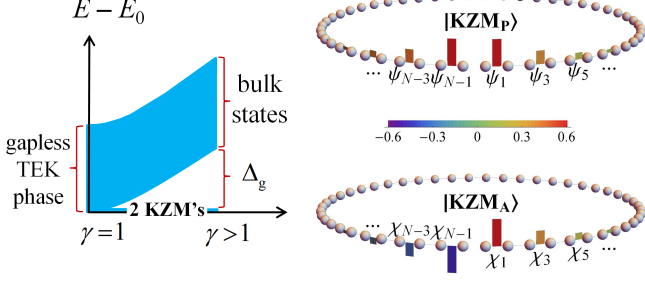


FIG. 5: (Color online) *Left*: The mechanism for the localized KZM's emerging within the gapless TEK phase. A gap, $\Delta_g = t(\gamma - 2 + 1/\gamma)$, develops when the bulk band is split by modulating the parameter $\gamma = t_N/t$ to the range, $\gamma > 1$. *Right*: Visualization of the two KZM's, $|KZM_P\rangle$ and $|KZM_A\rangle$. Here, we choose $N = 51, U = 1, t = 0.1$, and $\gamma = 2$ for demonstration. The coefficients, $\psi_2, \psi_4, \dots, \psi_{N-2}, \psi_N, \chi_2, \chi_4, \dots, \chi_{N-2}, \chi_N$, are not tagged because they are very small and neglectable.

Moreover, we can add more bond defects to tune the zero modes [37].

Summary and discussion.—In summary, a novel TEK phase and concomitant localized KZM's can be realized in the interacting Kitaev ring $H_R(c)$ with RF. According to the quaternary Jordan-Wigner mapping, this conclu-

sion is also true for the other three rings, $H_{NS}(c)$ and $H_{P/A}(\sigma)$ with odd number of lattice sites.

One may wonder why the gapless TEK phase can emerge in the interacting Hamiltonian $H_R(c)$, while not in the four auxiliary noninteracting Hamiltonians $H_{R/NS}^{(P)/(A)}(f)$. The answer lies in that their ground states are not valid ones with proper parity and should be filtered out according to the scheme in Fig. 2(b). So the valid states in their lowest upper band constitute the gapless spectra at low energies, which are exactly captured by the full quaternary Jordan-Wigner mapping.

Usually, the nontrivial topology is protected by a gap between the ground state and the bulk excitation spectra [38]. Here, the gapless TEK phase and concomitant KZM's do not comply with the convention for noninteracting fermionic systems. Also, the simultaneous occurring of nondegeneracy of the ground state and quadratic gapless spectra in a clean ring seems odd in the ordinary field theory [25].

Nowadays, state-of-the-art experimental platforms began to access these kind of theoretical models with flexible control methods [39–42]. The nontrivial TEK phase and versatile modulation of the KZM's mean such a system might be harvested in future quantum simulations.

We thank Yan He and Jian-Jun Dong for useful discussions. This work is supported by NSFC under Grants No. 11074177.

Appendix A: Exact solution of $H_R(c)$

According to the scheme depicted in Fig. 1(b), the solution of the Kitaev ring $H_R(c)$ is resort to the four free fermion Hamiltonians,

$$H_R^{(P)}(f) = H(1, -t + U, t + U), \quad (A1)$$

$$H_{NS}^{(P)}(f) = H(-1, -t + U, t + U), \quad (A2)$$

$$H_R^{(A)}(f) = H(1, t + U, -t + U), \quad (A3)$$

$$H_{NS}^{(A)}(f) = H(-1, t + U, -t + U). \quad (A4)$$

They can be cast into the general expression,

$$H(\xi, a, b) = \sum_{j=1}^{N-1} [a(f_j^\dagger f_{j+1} - f_j f_{j+1}^\dagger) + b(f_j^\dagger f_{j+1}^\dagger - f_j f_{j+1})] + \xi[a(f_N^\dagger f_1 - f_N f_1^\dagger) + b(f_N^\dagger f_1^\dagger - f_N f_1)] \quad (A5)$$

After Fourier transformation, we get

$$H(s, a, b) = \sum_{q \in Q_s, q \neq q_s} [2a \cos q(f_q^\dagger f_q - f_{-q} f_{-q}^\dagger) - 2ib \sin q(f_q^\dagger f_{-q}^\dagger - \text{h.c.})] + a \cos q_s(2f_{q_s}^\dagger f_{q_s} - 1), \quad (A6)$$

where s refers to R (or $\xi = 1$) or NS (or $\xi = -1$), $q_R = 0, q_{NS} = \pi$, and

$$Q_R = \{-\frac{N-1}{N}\pi, \dots, -\frac{2}{N}\pi, 0, \frac{2}{N}\pi, \dots, \frac{N-1}{N}\pi\}, \quad (A7)$$

$$Q_{NS} = \{-\frac{N-2}{N}\pi, \dots, -\frac{1}{N}\pi, \frac{1}{N}\pi, \dots, \frac{N-2}{N}\pi, \pi\}. \quad (A8)$$

By Bogoliubov transformation,

$$\eta_q = u_q f_q - i v_q f_{-q}^\dagger, \quad (q \neq 0, \pi), \quad (A9)$$

where

$$u_q^2 = \frac{1}{2} \left(1 + \frac{\epsilon(q)}{\omega(q)} \right), v_q^2 = \frac{1}{2} \left(1 - \frac{\epsilon(q)}{\omega(q)} \right),$$

$$2u_q v_q = \frac{D(q)}{\omega(q)}, \quad (\text{A10})$$

$$\epsilon(q) = a \cos q, D(q) = b \sin q, \quad (\text{A11})$$

$$\omega(q) = \sqrt{\epsilon(q)^2 + D(q)^2}, \quad (\text{A12})$$

we can diagonalize the fermionic Hamiltonian by arriving at

$$H(s, a, b) = \epsilon(q_s)(2f_{q_s}^\dagger f_{q_s} - 1) + \sum_{q \in Q_s, q \neq q_s} \omega(q) (2\eta_q^\dagger \eta_q - 1). \quad (\text{A13})$$

There are four fermion vacua in BCS-type wave functions,

$$|\phi_{\text{R/NS}}^{(\text{P})/(\text{A})}\rangle = \prod_{\substack{q \in Q_{\text{R/NS}}, \\ (0 < q < \pi)}} \left(u_q + i v_q f_q^\dagger f_{-q}^\dagger \right) |0\rangle \quad (\text{A14})$$

for $H_{\text{R/NS}}^{(\text{P})/(\text{A})}$ respectively. The two channels, $H_{\text{P/A}}(\sigma)$, provide two quasiparticle spectra,

$$\omega_{\text{P}}(q) = \sqrt{U^2 + t^2 - 2Ut \cos(2q)}, \quad (\text{A15})$$

$$\omega_{\text{A}}(q) = \sqrt{U^2 + t^2 + 2Ut \cos(2q)}. \quad (\text{A16})$$

The solution of $H_{\text{R}}(c)$ is obtained by filtering out redundant DOF by applying the scheme in Fig. 1 (b) backwards.

Of all the energy levels, we focus on the $2N$ extended-kink (EK) states. Half of them are of odd parity and form the spectrum,

$$E_{\text{P}}(q) = 2\omega_{\text{P}}(q) + \mathcal{E}_0 - (U - t), \quad (\text{A17})$$

while another half of them are of even parity and form the spectrum

$$E_{\text{A}}(q) = 2\omega_{\text{A}}(q) + \mathcal{E}_0 + |U + t| - 2U, \quad (\text{A18})$$

where

$$\mathcal{E}_0 = (U - t) - \sum_{q \in Q_{\text{R}}} \omega_{\text{P}}(q). \quad (\text{A19})$$

We should notice that the eigenstates of $H_{\text{R/NS}}^{(1)/(2)}$ are ones of the parity operator $\mathcal{P}_y = \exp(i\pi M_y)$ with $M_y = \sum_{j=1}^N f_j^\dagger f_j$, not the ones of parity operator \mathcal{P}_z . So a further projections by projectors $P_y^\pm = \frac{1}{2}(\hat{1} \pm \mathcal{P}_y)$ are needed. The validity of this route is ensued by the property (f -fermion particle-hole transformation),

$$\mathcal{C}_f^\dagger H_{\text{R}}^{(\text{P})/(\text{A})}(f) \mathcal{C}_f = H_{\text{NS}}^{(\text{P})/(\text{A})}(f), \quad (\text{A20})$$

$$\mathcal{C}_f = \prod_{j=1}^N [f_j^\dagger + (-1)^j f_j]. \quad (\text{A21})$$

This property means the energy levels of $H_{\text{R}}^{(\text{P})/(\text{A})}(f)$ and $H_{\text{NS}}^{(\text{P})/(\text{A})}(f)$ are the same. For example, in $H_{\text{P}}(\sigma)$ channel, the ground states of $H_{\text{R}}^{(\text{P})}(f)$ and $H_{\text{NS}}^{(\text{P})}(f)$ are $f_0^\dagger |\phi_{\text{R}}^{(\text{P})}\rangle$ and $|\phi_{\text{NS}}^{(\text{P})}\rangle$ respectively, i.e., they have the same energy value E_0 ,

$$H_{\text{R}}^{(\text{P})}(f) f_0^\dagger |\phi_{\text{R}}^{(\text{P})}\rangle = E_0 f_0^\dagger |\phi_{\text{R}}^{(\text{P})}\rangle, \quad (\text{A22})$$

$$H_{\text{NS}}^{(\text{P})}(f) |\phi_{\text{NS}}^{(\text{P})}\rangle = E_0 |\phi_{\text{NS}}^{(\text{P})}\rangle. \quad (\text{A23})$$

But their parities in y direction are opposite,

$$\mathcal{P}_y f_0^\dagger |\phi_{\text{R}}^{(\text{P})}\rangle = -f_0^\dagger |\phi_{\text{R}}^{(\text{P})}\rangle, \quad (\text{A24})$$

$$\mathcal{P}_y |\phi_{\text{NS}}^{(\text{P})}\rangle = +|\phi_{\text{NS}}^{(\text{P})}\rangle. \quad (\text{A25})$$

While \mathcal{P}_z is not diagonal in this subspace, $\{f_0^\dagger |\phi_{\text{R}}^{(\text{P})}\rangle, |\phi_{\text{NS}}^{(\text{P})}\rangle\}$. Because $\{\mathcal{P}_y, \mathcal{P}_z\} = 0$ and $\mathcal{P}_y^2 = \mathcal{P}_z^2 = 1$, we can find that

$$\mathcal{P}_z (f_0^\dagger |\phi_{\text{R}}^{(\text{P})}\rangle + |\phi_{\text{NS}}^{(\text{P})}\rangle) = +(f_0^\dagger |\phi_{\text{R}}^{(\text{P})}\rangle + |\phi_{\text{NS}}^{(\text{P})}\rangle), \quad (\text{A26})$$

$$\mathcal{P}_z (f_0^\dagger |\phi_{\text{R}}^{(\text{P})}\rangle - |\phi_{\text{NS}}^{(\text{P})}\rangle) = -(f_0^\dagger |\phi_{\text{R}}^{(\text{P})}\rangle - |\phi_{\text{NS}}^{(\text{P})}\rangle). \quad (\text{A27})$$

So the ground state with valid parity ($\mathcal{P}_z = -1$) reads

$$|E_0\rangle = |E_{\text{P}}(0)\rangle = \frac{1}{\sqrt{2}} (f_0^\dagger |\phi_{\text{R}}^{(\text{P})}\rangle - |\phi_{\text{NS}}^{(\text{P})}\rangle). \quad (\text{A28})$$

The upper EK states can be treated in the subspaces of the same energy value likewise. We finally get ($q \in Q_{\text{R}}$)

$$|E_{\text{P}}(q)\rangle = \frac{1}{\sqrt{2}} \left(\eta_q^\dagger |\phi_{\text{R}}^{(\text{P})}\rangle - \eta_{\pi-q}^\dagger f_\pi^\dagger |\phi_{\text{NS}}^{(\text{P})}\rangle \right), \quad (\text{A29})$$

$$|E_{\text{A}}(q)\rangle = \frac{1}{\sqrt{2}} \left(\eta_q^\dagger |\phi_{\text{R}}^{(\text{A})}\rangle + \eta_{\pi-q}^\dagger f_\pi^\dagger |\phi_{\text{NS}}^{(\text{A})}\rangle \right), \quad (\text{A30})$$

$$|E_{\text{A}}(0)\rangle = \frac{1}{\sqrt{2}} \left(f_0^\dagger |\phi_{\text{R}}^{(\text{A})}\rangle + |\phi_{\text{NS}}^{(\text{A})}\rangle \right). \quad (\text{A31})$$

For finite N , in the range $t > 0$ and $-\infty < U < \infty$, the non-degenerate ground state is always $|E_{\text{P}}(0)\rangle$. In the thermodynamic limit, the sum can be replaced by an integral and leads to per site ground state energy,

$$E_0/N = -\frac{2|U+t|}{\pi} E \left(\frac{4Ut}{(U+t)^2} \right), \quad (\text{A32})$$

where $E(x)$ is the complete elliptic integral of the second kind. The second derivatives of E_0/N at the points $U = \pm t$ are divergent, which signifies phase transition points.

The density of states (DOS) near the ground state can be worked out by $E_{\text{P/A}}(q)$ rigorously and reads

$$\rho(x) = \frac{2[x + 2(U-t)]}{\pi \sqrt{x(x+4U)(4t-x)[x+4(U-t)]}}. \quad (\text{A33})$$

where $x = E - E_0$. It is divergent at low energies,

$$\rho(x) \sim ax^{-\frac{1}{2}} + bx^{\frac{1}{2}} + O(x^{\frac{3}{2}}), \quad (\text{A34})$$

$$a = \frac{(U-t)^{1/2}}{2\pi(Ut)^{1/2}}, \quad (\text{A35})$$

$$b = \frac{U^2 + Ut + t^2}{16\pi(Ut)^{3/2}(U-t)^{1/2}}. \quad (\text{A36})$$

Appendix B: Correlation function of the ground state

The correlation function is defined as

$$\begin{aligned} C_{r,N} &= \langle E_P(0) | (2n_j - 1)(2n_{j+r} - 1) | E_P(0) \rangle \\ &= \langle E_P(0) | \sigma_j^z \sigma_{j+r}^z | E_P(0) \rangle. \end{aligned} \quad (B1)$$

Due to the parity, we have $\langle \phi_R^{(P)} | f_0 \sigma_j^z \sigma_{j+r}^z | \phi_{NS}^{(P)} \rangle = 0$. By introducing the Majorana fermions,

$$A_l = f_l^\dagger + f_l, B_l = f_l^\dagger - f_l, \quad (B2)$$

we can expand the product of two spin operators as

$$\sigma_j^z \sigma_{j+r}^z = B_j A_{j+1} B_{j+1} \dots A_{j+r-1} B_{j+r-1} A_{j+r}. \quad (B3)$$

Then by using Wick's theorem basing on the relations,

$$\begin{aligned} \langle f_0 f_0^\dagger \rangle &= 1, \\ \langle A_j f_0^\dagger \rangle &= -\langle B_j f_0^\dagger \rangle = \frac{1}{\sqrt{N}}, \\ \langle A_i A_j \rangle &= -\langle B_i B_j \rangle = \delta_{i,j}, \\ \langle B_i A_{i+r} \rangle &= -\langle A_{i+r} B_i \rangle = \mathcal{D}_{r+1}^{(s)}, \end{aligned} \quad (B4)$$

we get the Toeplitz determinant representation of the correlation function,

$$\begin{aligned} C_{r,N} &= \frac{1}{2} (\langle \phi_R^{(P)} | f_0 \sigma_j^z \sigma_{j+r}^z f_0^\dagger | \phi_R^{(P)} \rangle + \langle \phi_{NS}^{(P)} | \sigma_j^z \sigma_{j+r}^z | \phi_{NS}^{(P)} \rangle) \\ &= \frac{1}{2} \left(\begin{vmatrix} \mathcal{D}_0^{(R)} + \frac{2}{N} & \mathcal{D}_{-1}^{(R)} + \frac{2}{N} & \dots & \mathcal{D}_{1-r}^{(R)} + \frac{2}{N} \\ \mathcal{D}_1^{(R)} + \frac{2}{N} & \mathcal{D}_0^{(R)} + \frac{2}{N} & \dots & \mathcal{D}_{2-r}^{(R)} + \frac{2}{N} \\ \dots & \dots & \dots & \dots \\ \mathcal{D}_{r-1}^{(R)} + \frac{2}{N} & \mathcal{D}_{r-2}^{(R)} + \frac{2}{N} & \dots & \mathcal{D}_0^{(R)} + \frac{2}{N} \end{vmatrix} + \begin{vmatrix} \mathcal{D}_0^{(NS)} & \mathcal{D}_{-1}^{(NS)} & \dots & \mathcal{D}_{1-r}^{(NS)} \\ \mathcal{D}_1^{(NS)} & \mathcal{D}_0^{(NS)} & \dots & \mathcal{D}_{2-r}^{(NS)} \\ \dots & \dots & \dots & \dots \\ \mathcal{D}_{r-1}^{(NS)} & \mathcal{D}_{r-2}^{(NS)} & \dots & \mathcal{D}_0^{(NS)} \end{vmatrix} \right) \\ &= \frac{1}{2} \left(\det[\mathcal{D}_{l-m}^{(R)} + \frac{2}{N}]_{1 \leq l, m \leq r} + \det[\mathcal{D}_{l-m}^{(NS)}]_{1 \leq l, m \leq r} \right), \end{aligned} \quad (B5)$$

where

$$\begin{aligned} \mathcal{D}_n^{(s)} &= -\frac{e^{-iq_s}}{N} e^{-iq_s n} + \frac{1}{N} \sum_{q \in Q_s, q \neq q_s} e^{-iqn} D(e^{iq}), \\ D(e^{iq}) &= -\frac{U - te^{2iq}}{\sqrt{(U - te^{2iq})(U - te^{-2iq})}}. \end{aligned} \quad (B6)$$

The Toeplitz determinants can be evaluated numerically for quite a large system. In the thermodynamic limit, we can analyse the asymptotic behavior of the correlation function with a generalized Szegő's theorem and obtain

[23, 24, 27]

$$\begin{aligned} C(r, \alpha) &\equiv \lim_{N \rightarrow \infty} C_{r,N} \\ &\approx \begin{cases} \sqrt{1 - t^2/U^2}, & (U < -t), \\ 0, & (|U| < t), \\ (-1)^r (1 - 2\alpha) \sqrt{1 - t^2/U^2}, & (U > t), \end{cases} \end{aligned} \quad (B7)$$

where $\alpha = \frac{r}{N}$.

-
- [1] L. Fidkowski and A. Kitaev, Phys. Rev. B **81**, 134509 (2010); *ibid.* **83**, 075103 (2011).
 - [2] A.M. Turner, F. Pollmann, and E. Berg, Phys. Rev. B **83**, 075102 (2011).
 - [3] A. Rahmani, X. Zhu, M. Franz, and I. Affleck, Phys.

- Rev. Lett. **115**, 166401 (2015); Phys. Rev. B **92**, 235123 (2015).
- [4] H. Katsura, D. Schuricht, and M. Takahashi, Phys. Rev. B **92**, 115137 (2015).
- [5] J. Wouters, H. Katsura, and D. Schuricht, Phys. Rev. B

- 98**, 155119 (2018).
- [6] A.P. Schnyder, S. Ryu, A. Furusaki, and A. W. W. Ludwig, Phys. Rev. B **78**, 195125 (2008).
 - [7] A.Y. Kitaev, AIP Conf. Proc. **1134**, 22 (2009).
 - [8] J.-J. Miao, H.-K. Jin, F.-C. Zhang, and Y. Zhou, Phys. Rev. Lett. **118**, 267701 (2017); Sci. Rep. **8**, 488 (2018).
 - [9] M. Ezawa, Phys. Rev. B **96**, 121105(R) (2017).
 - [10] Y. Wang, J.-J. Miao, H.-K. Jin, and S. Chen, Phys. Rev. B **96**, 205428 (2017).
 - [11] G. Y. Chitov, Phys. Rev. B **97**, 085131 (2018).
 - [12] H. T. Diep, *Frustrated Spin Systems* (World Scientific, Singapore, 2004).
 - [13] C. M. Dawson and M. A. Nielsen, Phys. Rev. A **69**, 052316 (2004).
 - [14] A. Ferraro, A. García-Saenz, and A. Acín, Phys. Rev. A **76**, 052321 (2007).
 - [15] S. M. Giampaolo, G. Adesso, and F. Illuminati, Phys. Rev. Lett. **104**, 207202 (2010).
 - [16] S.M. Giampaolo, G. Gualdi, A. Monras, and F. Illuminati, Phys. Rev. Lett. **107**, 260602 (2011).
 - [17] U. Marzolino, S. M. Giampaolo, and F. Illuminati, Phys. Rev. A **88**, 020301(R) (2013).
 - [18] S. M. Giampaolo, B. C. Hiesmayr, and F. Illuminati, Phys. Rev. B **92**, 144406 (2015).
 - [19] W. Nie, H. Katsura, and M. Oshikawa, Phys. Rev. B **97**, 125153 (2018).
 - [20] R. Z. Bariev, Zh. Eksp. Teor. Fiz. **77**, 1217 (1979) [Sov. Phys. JETP **50**, 613 (1979)].
 - [21] G. G. Cabrera and R. Jullien, Phys. Rev. Lett. **57**, 393 (1986); Phys. Rev. B **35**, 7062 (1987).
 - [22] M. Campostrini, A. Pelissetto, and E. Vicari, Phys. Rev. E **91**, 042123 (2015); J. Stat. Mech. (2015) P11015.
 - [23] J.-J. Dong, P. Li, and Q.-H. Chen, J. Stat. Mech. (2016) 113102.
 - [24] J.-J. Dong, Z.-Y. Zheng, and P. Li, Phys. Rev. E **97**, 012133 (2018).
 - [25] S. M. Giampaolo, F. B. Ramos, and F. Franchini, arXiv:1807.07055.
 - [26] Y. He and H. Guo, J. Stat. Mech. (2017) 093101.
 - [27] P. Li and Y. He, Phys. Rev. E **99**, 032135 (2019).
 - [28] E. Lieb, T. Schultz and D. C. Mattis, Ann. of Phys. **16**, 407 (1961).
 - [29] P. Di Francesco, P. Mathieu, D. Senechal, *Conformal Field Theory* (Springer-Verlag, New York, 1997).
 - [30] The spin ring is called an "a-cyclic" problem in [28].
 - [31] J.-J. Dong and P. Li, Mod. Phys. Lett. B **31**, 1750061 (2017).
 - [32] C. N. Yang, Phys. Rev. **85**, 808 (1952).
 - [33] A. Y. Kitaev, Phys. Usp. **44**, 131 (2001).
 - [34] K. Kawabata, R. Kobayashi, N. Wu, and H. Katsura, Phys. Rev. B **95**, 195140 (2017).
 - [35] T. Giamarchi, *Quantum Physics in One Dimension* (Oxford University Press, Oxford, 2003).
 - [36] C. Yin, H. Jiang, L. Li, R. Lü, and S. Chen, Phys. Rev. A **97**, 052115 (2018).
 - [37] More versatile modulation will be reported elsewhere (in preparing).
 - [38] S.-Q. Shen, *Topological Insulators* (Springer, Berlin, 2012).
 - [39] H. Labuhn, D. Barredo, S. Ravets, S. de Léséleuc, T. Macrì, T. Lahaye, and A. Browaeys, Nature **534**, 667 (2016).
 - [40] H. Bernien, S. Schwartz, A. Keesling, H. Levine, A. Omran, H. Pichler, S. Choi, A. S. Zibrov, M. Endres, M. Greiner, V. Vuletic, and M. D. Lukin, Nature **551**, 579 (2017).
 - [41] E. Guardado-Sanchez, P. T. Brown, D. Mitra, T. Devakul, D. A. Huse, P. Schauß, and W. S. Bakr, Phys. Rev. X **8**, 021069 (2018).
 - [42] V. Lienhard, S. de Léséleuc, D. Barredo, T. Lahaye, and A. Browaeys, Phys. Rev. X **8**, 021070 (2018).